ELSEVIER

Computational Materials Science 29 (2004) 419–427

COMPUTATIONAL MATERIALS SCIENCE

www.elsevier.com/locate/commatsci

A study on the metal flow in full penetration laser beam welding for titanium alloy

Hanbin Du *, Lunji Hu, Jianhua Liu, Xiyuan Hu

School of Materials Science & Engineering, Huazhong University of Science & Technology, Wuhan 430074, China

Received 12 May 2003; received in revised form 20 October 2003; accepted 28 November 2003

Abstract

A mathematical model for flow simulation of full penetration laser beam welding of titanium alloy is presented. In this model, the heat source comprises a plane heat source on the top surface and a cylindrical heat source along the *z*-direction, which takes into account the plasma effect and the keyhole absorption. By solving the conservation equations of energy, momentum and mass, the temperature and flow fields are obtained. The momentum interpolation scheme with under-relaxation parameter is used to simplify the calculation algorithm and save the storage space of computer. The mushy region is introduced to provide a simple method to dispose of the pressure and velocity boundary conditions. Results calculated from the models are found to agree with the experimental results for the geometry profile of weld. The calculated results indicate the metal flow is the main reason for forming the typical ''hourglass'' cross-section profile.

Keywords: Laser beam welding; Titanium alloy; Flow field; Momentum interpolation; Simulation; Finite-difference

1. Introduction

In recent years, various models have been developed in order to explain the main mechanisms arising in deep penetration laser welding. Previously, a two-dimensional model was used by Sluzalec [1] to study the flow of metal subjected to a laser beam, in which changes of the laser beam intensity in time was taken into account. Afterward, models began to pay attention to vaporizing effect and keyhole formation [2]. The complexity arising from the laser–matter energy coupling at high power intensities led researchers to study different aspects in detail separately: thermo-capillary flow and the influence of alloy elements, polarization of the laser beam, plasma absorption within the keyhole and shielding gas effects associated with formation of a plasma plume outside the specimen [3–9]. Together with these particular studies, some authors developed integrated models in order to keep a complete vision of the whole problem [5,8]. A three-dimensional model was developed by Ye [6] to study the heat transfer and fluid flow in the laser full-penetration welding. But, all of the models mainly focused on the study on the steel materials or aluminum alloys. No model was founded to

* Corresponding author. Tel.: +86-27-87543894; fax:+86-27-87543776.

E-mail address: dhbcll@hotmail.com (H. Du).

0927-0256/$ - see front matter © 2003 Elsevier B.V. All rights reserved.
doi:10.1016/j.commatsci.2003.11.002

predict the weld profile of the laser weld for titanium alloy. With the special materials properties, the weld geometry of titanium alloys appears difference characters with other materials. A thorough investigation of flow in the weld pool can meet the needs for exactly controlling the profile of the weld, which is very important for the titanium alloy products used in the aerospace and aviation industries.

In this paper, we present an analysis of metal flow in the laser welded molten pool. In order to accurately simulate the weld profile, the keyhole absorption and plasma effect is taken into account. A plane heat source on the top surface and a cylindric heat source along laser beam axis are used to consider this effect.

In the past, the staggered grid technology was used to get the correct velocity–pressure coupling. In a staggered grid system there are three distinct nodes and control volumes associated with the same index label. The nodal staggering complicates the programming and implementation of the solution algorithm. Clearly, it would be beneficial if one could discretize the governing equations using a grid system that places the entire flow variables at the same physical location. Unfortunately the use of such a nonstaggered grid system with a primitive variable formulation of the incompressible equations has been shown to produce nonphysical oscillations in the pressure field. These spatial oscillations occur when one applies central differencing to both the continuity equations and the pressure gradient term in the momentum equations. In this paper, the momentum interpolation scheme is introduced based on nonstaggered grid technology. It can effectively eliminate the pressure oscillations by the momentum interpolation for velocities and linear interpolation for pressure.

Another difficulty in flow simulation is to dispose the pressure and velocity boundary conditions on the interface of solid–liquid phase transformation. In the past, the phase transformation process was always assumed an isothermal one. A mushy region is introduced in this model. On one hand, the solid–liquid phase transformation is considered to happen in a range, instead of at a point. On the other hand, it is useful to deal with the trouble related to the pressure and velocity boundary conditions.

2. The model

The welding process is supposed to occur in a quasi-stationary way, in Cartesian co-ordinates with its origin at the center of the laser source at the specimen bottom surface. The model is shown in Fig. 1. In order to set up a tractable model, the surface of the molten pool is assumed to be flat. The form and size of the molten pool in laser beam welding will adjust themselves according to external conditions such as material, laser power and traveling speed. The domain of flow is the region which temperature exceeds the melting point. So, the heat conduction equation must be solved at first. Then, by solving the momentum and pressure equations, the flow velocity is assured. At last, considering the influence of metal flow in the weld pool, the melting point isothermal is reascertained by solving the energy equation. A numerical finite-difference method is applied to solve the three-dimensional heat conduction and flow problem.

2.1. Control equation

The fundamental equations and boundary conditions are expressed below. The base equation reads

$$\rho c\left((u-u_0)\frac{\partial T}{\partial x}+v\frac{\partial T}{\partial y}+w\frac{\partial T}{\partial z}\right)=\frac{\partial}{\partial x}\left(\lambda\frac{\partial T}{\partial x}\right)+\frac{\partial}{\partial y}\left(\lambda\frac{\partial T}{\partial y}\right)+\frac{\partial}{\partial z}\left(\lambda\frac{\partial T}{\partial z}\right)+Q \tag{1}$$

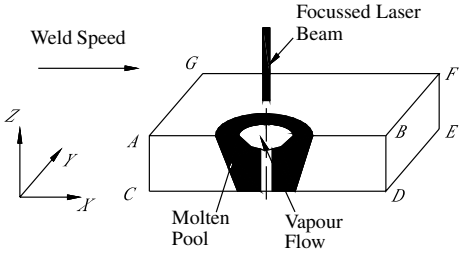

Fig. 1. The model for computation of the flow field.

$$\rho\left((u-u_0)\frac{\partial u}{\partial x}+v\frac{\partial u}{\partial y}+w\frac{\partial u}{\partial z}\right)=-\frac{\partial P}{\partial x}+\mu\left(\frac{\partial^2 u}{\partial x^2}+\frac{\partial^2 u}{\partial y^2}+\frac{\partial^2 u}{\partial z^2}\right) \tag{2a}$$

$$\rho\left((u-u_0)\frac{\partial v}{\partial x}+v\frac{\partial v}{\partial y}+w\frac{\partial v}{\partial z}\right)=-\frac{\partial P}{\partial y}+\mu\left(\frac{\partial^2 v}{\partial x^2}+\frac{\partial^2 v}{\partial y^2}+\frac{\partial^2 v}{\partial z^2}\right) \tag{2b}$$

$$\rho\left((u-u_0)\frac{\partial w}{\partial x}+v\frac{\partial w}{\partial y}+w\frac{\partial w}{\partial z}\right)=F_z-\frac{\partial P}{\partial z}+\mu\left(\frac{\partial^2 w}{\partial x^2}+\frac{\partial^2 w}{\partial y^2}+\frac{\partial^2 w}{\partial z^2}\right) \tag{2c}$$

$$\frac{\partial u}{\partial x}+\frac{\partial v}{\partial y}+\frac{\partial w}{\partial z}=0 \tag{3}$$

where $F_z=-\rho\beta g(T-T_0)$, ρ is density, T temperature, T_0 the reference temperature (the melting temperature), c specific heat, β expansion coefficient of volume, g acceleration due to gravity, λ heat conductivity, μ viscosity, P pressure, u, v, w the fluid velocities along x, y, z directions, u_0 the welding speed, Q heat source intensity per volume.

2.2. The heat source submodel

In laser beam welding the energy is absorbed by the material and converted into heat. The process of laser deep penetration welding is characterized by the existence of plasma and a keyhole. The plasma is formed by ionized metal vapor which temperature can reach 20 000 °C [10]. It is like a moving heat source along with the molten pool, which leads to the wider molten pool at the top section of the weld. At the same time, the laser energy is transferred to the keyhole wall either by the plasma or by direct absorption at the keyhole wall. During the computation, it is considered that the heat source comprises a plane heat source on the top surface and a cylindrical heat source along the z-direction. On the basis of experimental observations, 25% of the heat power is absorbed on the surface of the specimen (Q_{surf}), 75% by the keyhole wall (Q_{bottom}) [10]. The former is coupled to the energy equation by heat flux boundary condition, the latter coupled by the heat source intensity of volume.

Assuming the laser beam maintains a constant TEM_{00} mode, the Gaussian power distribution $q(x,y)$ can be expressed as:

$$q(x,y)=q_{\text{m}}\exp\left(-\frac{3(x^2+y^2)}{R^2}\right) \tag{4}$$

where q_{m} is the maximum heat flux per unit area and R is the heat source effective radius ($R=2\times r_0$, r_0 is the average keyhole radius, about 0.3 mm) [5]. q_{m} can be expressed as:

$$q_{\text{m}}=\frac{3}{\pi R^2}Q_{\text{surf}} \tag{5}$$

Assuming the laser energy is uniformly absorbed on the wall of the keyhole. Therefore, the Q can be expressed as:

$$Q=\frac{Q_{\text{bottom}}}{\pi r_0^2 h} \tag{6}$$

where h is the plate thickness.

2.3. The heat boundary condition

On the top surface the heat boundary condition is

$$-\lambda\frac{\partial T}{\partial r}=\begin{cases}q & r\leqslant r_0\\ h_{\text{f}}(T-T_{\text{a}}) & r>r_0\end{cases} \tag{7}$$

where h_{f} is the coefficient of heat emission, T_{a} is the environment temperature, and q is the heat flux per unit area.

On the other surface of the model, the heat boundary condition is

$$-\lambda\frac{\partial T}{\partial i}=h_{\text{f}}(T-T_{\text{a}})\quad(i=x,y,z) \tag{8}$$

A half of the work-piece is used for calculation. According to symmetry, on the face ABCD in Fig. 1, the energy meets the adiabatic condition:

$$\frac{\partial T}{\partial y}=0 \tag{9}$$

2.4. The flow boundary condition

At the top and bottom of the weld pool, the liquid metal flow under surface tension, the velocity equation can be expressed by

$$\mu\frac{\partial u}{\partial z} = -\frac{\partial \sigma}{\partial T}\frac{\partial T}{\partial x} \tag{10a}$$

$$\mu\frac{\partial v}{\partial z} = -\frac{\partial \sigma}{\partial T}\frac{\partial T}{\partial y} \tag{10b}$$

$$w = 0 \tag{10c}$$

where σ is surface tension.

Because the liquid metal cannot pass through the symmetry face, the boundary condition on the symmetry face can be expressed by

$$\frac{\partial u}{\partial y} = \frac{\partial v}{\partial y} = 0 \tag{11}$$

In the past, as the liquid region turned into solid, it was always used the zero velocity condition on the interface of the solid and liquid. In fact, these applications assume that liquid–solid phase transformation occurs in a pure material. In many practical situations, however, the material under consideration is not pure. In such cases the phase transformation takes place over a temperature range. That is, the evolution of latent heat has a functional relationship with the temperature, as opposed to the step change associated with an isothermal phase transformation. Problems of this type are often referred to as mushy region problems to indicate the solid plus liquid state of the material in the phase transformation range [10].

Assuming the phase transformation temperature range is $2\Delta T$, and the quantity ΔT is referred to as the half temperature range of the mushy zone. The task of fully defining nature of the latent heat evolution in the mushy region is that of identifying the form of the local solid fraction–temperature relationship, i.e. $F_s(T)$. A simple linear form is chosen [11]

$$F_s(T) = \begin{cases} 0 & T \geqslant T_0 + \Delta T \\ (\Delta T + T_0 - T)/2\Delta T & T_0 + \Delta T > T \geqslant T_0 - \Delta T \\ 1 & T < T_0 - \Delta T \end{cases} \tag{12}$$

where $T_0 = (T_S + T_L)/2$, T_S is the start temperature of solid–liquid phase transformation and T_L the end temperature of that.

In order to deal with the mushy problem, a source term has been added to right side of the momentum equation. The S_x, S_y and S_z source terms are used to modify the momentum equations in the mushy region. As the liquid scale decreases, the velocity also decreases, down to 0 when the mush becomes a complete solid. In a numerical model this behavior can be accounted for by defining

$$S_x = Au, \quad S_y = Av \quad \text{and} \quad S_z = Aw \tag{13}$$

where A increase from 0 to a large value as the local solid fraction F_s increases from its liquid value of 0 to its solid value of 1. According the Carman–Koseny equation [11], the above A in equation can be expressed as

$$A = -C(1-k)^2/(k^3 + q) \tag{14}$$

where

$$k = 1 - F_s(T) \tag{14a}$$

In the current study, C is assumed constant and is set to 1.6×10^3. The constant q, introduced to avoid division by 0, is set at 0.001. In this way, it is an advantage that the liquid and solid zones can be solved as a whole. Except for the symmetry face and the top and bottom surface, zero velocity condition is set on the other boundaries of the calculation domain.

3. The basic numerical solution

The solution of the governing Eqs. (1)–(3) with the boundary conditions is carried out numerically by means of a finite differential method with a nonuniform gridspacing.

3.1. Mesh subdivision of the model

In laser welding, an important factor influencing the metal flow is the surface tension. Due to the surface tension only acts on the surface of the weld pool, the flow driven by the surface tension pro-

duces thin velocity boundary. Chen provides the scale of this variable [12]

$$\delta_v = \sqrt{\upsilon w/U_s} \tag{15}$$

where $\upsilon = \mu/\rho$, is the kinematics viscosity, w is the width of the weld melt, U_s is the characterized velocity.

Under the typical laser beam welding condition, the surface flow boundary is smaller than 10^{-4} m. In order to calculate the flow in the weld pool accurately, the grid near the surface must be smaller than δ_v. In the middle of plates, the grid is coarser than near the surface.

Similarly, nonuniform grid system is also used along the x and y direction. The grid model is showed in Fig. 2.

3.2. The discretization form

The finite-difference discretization, following the notation in Patankar [13] and referring to Fig. 3, gives

$$a_p\phi_p = a_E\phi_E + a_W\phi_W + a_N\phi_N + a_S\phi_S + a_T\phi_T + a_B\phi_B + b \tag{16}$$

where the subscripts indicate the surrounding nodal values, the a's are coefficients which depend on the diffusion and convective fluxes into the pth control volume. The parameter b incorporates a discretized form of the source term S. The energy equation, the momentum equations and the continuity equation keep the common discretized form. Significations of the denotations are listed in Table 1.

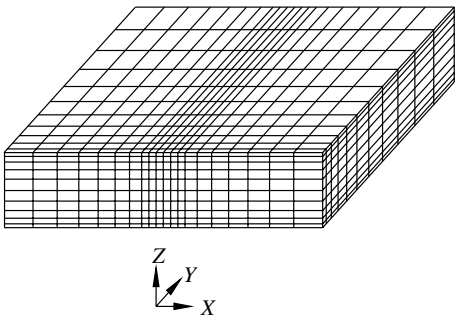

Fig. 2. Mesh subdivision of the model.

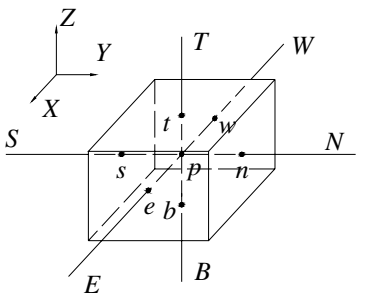

Fig. 3. The discretization control cell.

Table 1
Signification of the denotations

Control equations	Parameter Φ	Coefficients a	Source term
x momentum equation	u	μ	$\partial P/\partial x + Au$
y momentum equation	v	μ	$\partial P/\partial y + Av$
z momentum equation	w	μ	$F_z - \partial P/\partial z + Aw$
Continuity equation	1	0	0
Energy equation	T	λ/c	0

3.3. The momentum interpolation scheme

In the nonstaggered arrangement for the momentum equations one needs interpolation to obtain cell face velocities for convective flux calculation and also to obtain cell face pressures for evaluation of the pressure gradient. For the continuity equation, however, the interpolation is needed only to obtain cell face velocities for evaluation of the mass imbalance. Majumdar [14] had successfully used linear interpolation for pressure and momentum interpolation for velocities to solve the flow field.

The momentum interpolation scheme for two adjacent one-dimensional control volumes in the nonstaggered arrangement gives:

$$u_{i+1/2} = [f^+h_{i+1} + (1-f^+)h_i] + \frac{wD_v^{i+1/2}}{\overline{a}_p}(P_i - P_{i+1}) + (1-w)[u^*_{i+1/2} - f^+u^*_{i+1} - (1-f^+)u^*_i] \tag{17}$$

where

$$h_i = u_i - \frac{wD_v^i}{a_p^i}(P_{i-1/2} - P_{i+1/2}) \tag{17a}$$

$$h_{i+1} = u_{i+1} - \frac{wD_v^{i+1}}{a_p^{i+1}}(P_{i+1/2} - P_{i+3/2}) \tag{17b}$$

$$\frac{1}{\overline{a}_p} = \frac{f^+}{a_p^{i+1}} + \frac{1-f^+}{a_p^i} \tag{17c}$$

$$f^+ = Pe/(Pe + eE) \tag{17d}$$

$u_{i+1/2}$ is velocity on the right of cell face, Var* are values of variable at the previous iteration level, a_p value is listed as Eq. (15), ω is the under-relax factor. u_i is referred to the i node x-direction velocity, and $D_v^{i+1/2}$ is the control volume face area, P_i is the ith node pressure value, and f is the geometric interpolation factor, Pe, eE as showed in Fig. 3.

3.4. The convergence rule and the flow chart

The computation of temperature field and velocity field must accord with the convergence rule:

$$\mathrm{Max}(|\phi_i^{n+1} - \phi_i^n|)/\phi_i^{n+1} \leqslant 10^{-3} \tag{18}$$

The calculation chart is shown in Fig. 4.

4. Results and discussion

The described algorithm has then been implemented on VC++ platform. The model size is 100 mm × 100 mm × 1.5 mm, the mesh grids are 256 × 128 × 22. The used reference properties of the materials of the molten zone are given in Table 2.

Fig. 5 shows the isotherm of the T_0 temperature of TC1 titanium alloy on the top surface, without consideration of the Marangoni effect. TC1 is a kind of titanium alloy produced by vacuum arc furnace melting according to the Chinese Standard GB6613-83. Fig. 6 shows the isotherm of that with consideration of the Marangoni effect. Comparing the two figures, we can find the molten pool becomes shorter and wider with the Marangoni effect. It indicates that the Marangoni flow plays an important role in transferring the heat from the center of laser beam to the molten boundary. The heat is quickly transferred to the solid–liquid boundary of welded pool, therefore, the weld pool become wider just like the heat conductivity greatly increases. At the same time, the molten metal in the rear of pool becomes cooled and solidified more quickly due to the heat is dissipated. So the pool becomes shorter with the Marangoni effect than without considering the Marangoni effect.

Fig. 7 shows the molten pool profile of the transverse section. Undergoing the surface heat source on the top surface and the cylindric heat source along the laser beam axial direction, a keyhole is formed in the weld pool. But the simulation without considering flow effect does not predict the weld pool profile in agreement with the experiment measurement. Especially, the calculated weld pool widths are too small.

What is more important for laser beam welding of titanium is the influence of surface tension gradients. The left side of Fig. 8 shows the transverse section with a negative temperature coefficient of surface tension, the metal flows from the higher-temperature keyhole boundary to the lower-temperature molten pool boundary and this leads to an expansion of the fusion zone at the top and the bottom surface. The whole profile of the weld metal is hourglass shape, which means that the top is the widest, the bottom narrower, and the middle the narrowest. It indicates that the metal flow is the main reason to form the typical profile of laser welding.

A comparison of the geometry of the weld pool established experimentally with that calculated according to the above model is presented in Fig. 8. The two profiles coincide quite well.

Fig. 9 shows the flow circulation of the metal in the molten pool. During the flow computation, the region which temperature was over the vaporization point was considered as a part of the flow domain. In this way, the energy absorbed by plasma in the keyhole can be transferred to the molten pool. It also shows the convection circulation forms in the molten pool with a negative temperature coefficient of surface tension. The maximum flow velocity appears on the surface of

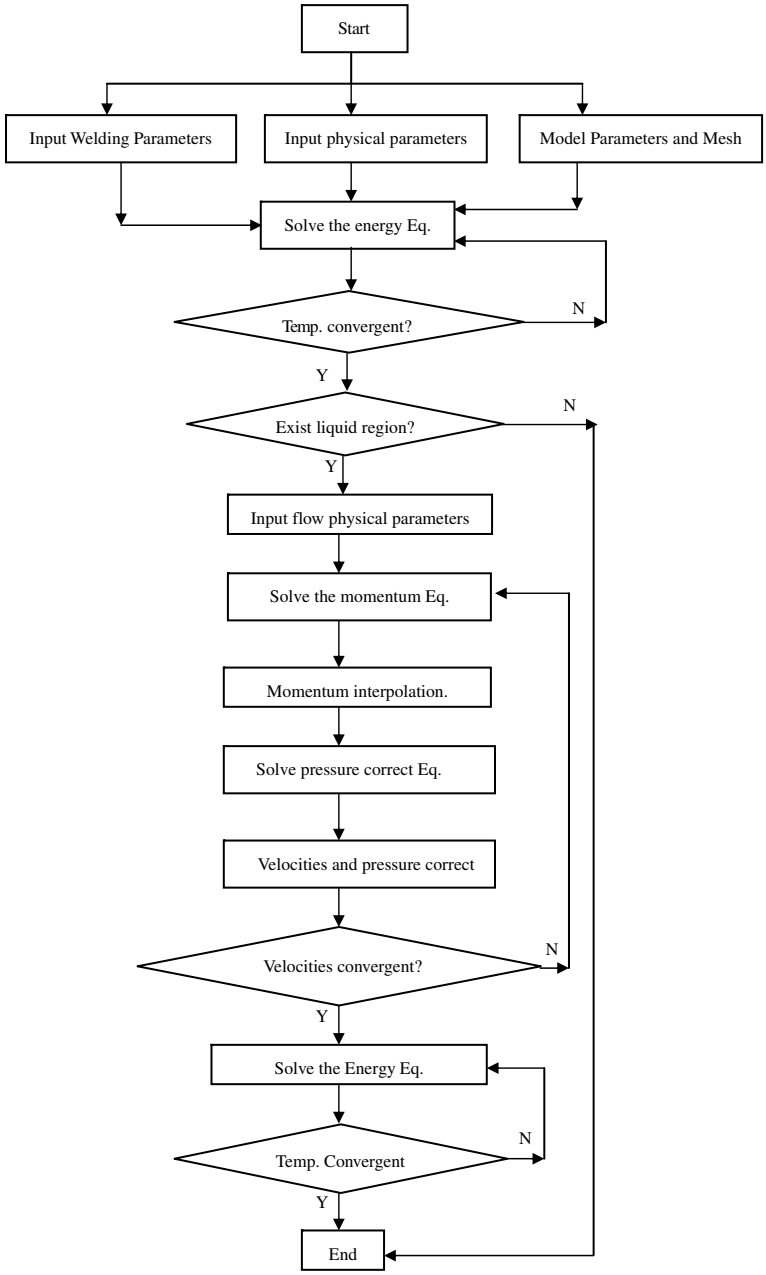

Fig. 4. Flow chart of the calculation.

molten pool where there is the maximum temperature gradient. The liquid metal flows from the center of the laser beam to the molten pool boundary. This leads to an expansion of the fusion zone in the top and bottom surface areas.

5. Conclusions

(1) A comprehensive fluid flow and the combinated heat sources model is developed to simulate the geometry profile of the weld of laser

Table 2
Material properties of liquid metal at reference temperatures

Temperature (K)	293	373	473	573	673	773
Heat conductivity, λ ($W\,m^{-1}\,K^{-1}$)	9.63	10.47	11.72	12.14	13.40	14.65
Specific heat capacity, c ($J\,kg^{-1}\,K^{-1}$)	–	574	–	641	699	729
Liquid metal density, ρ ($kg\,m^{-3}$)	4200					
Expansion coefficient of volume, β (K^{-1})	1.0×10^{-4}					
Surface tension gradient, $\partial\sigma/\partial T$ ($kg\,s^{-2}\,K^{-1}$)	-0.35×10^{-4}					
Kinematics viscosity, υ ($m^2\,s^{-1}$)	1.05×10^{-5}					
The transformation start temperature, T_S (K)	1743					
The boiling temperature, T_B (K)	3557					
The transformation end temperature, T_L (K)	1813					
The ambient temperature, T_a (K)	293					

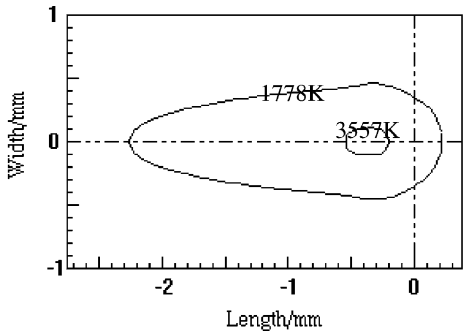

Fig. 5. The molten pool profile on the top surface without considering Marangoni effect.

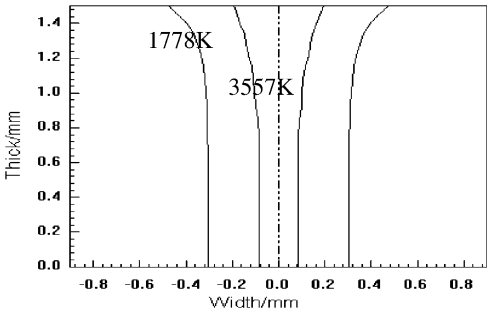

Fig. 7. The keyhole and molten pool under the combined heat source.

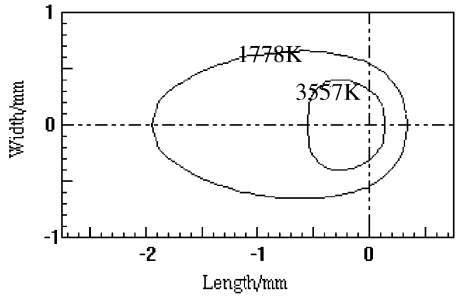

Fig. 6. The molten pool profile on the top surface with considering Marangoni effect.

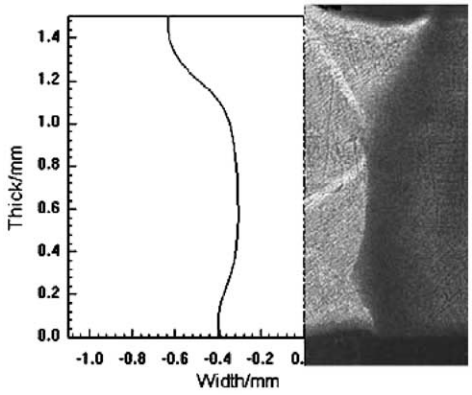

Fig. 8. Comparison of weld formation in laser beam welding determined experimentally with that by calculation.

beam welding of titanium alloys. The Results calculated from the model were found to agree with the experimental results for the geometry profile of weld.

(2) The calculated results showed that the molten pool becomes shorter and wider with the Marangoni effect. It also indicated that the metal flow is the main reason for forming the typical "hourglass" cross-section profile.

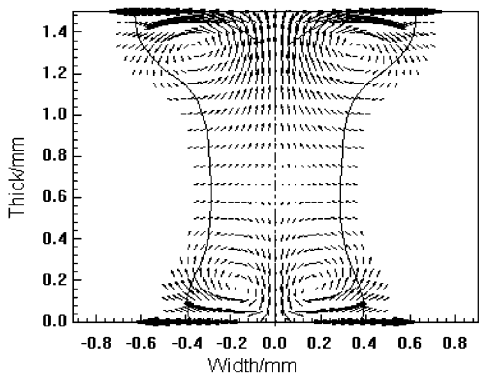

Fig. 9. The velocity distribution in the weld pool.

(3) It is confirmed that the momentum interpolation system with under-relaxation parameter based on nonstaggered grid technology can effectively eliminate the pressure oscillations. In this way, high accuracy results can be achieved with a less computer time and storage space.
(4) The methodology for the modeling of mushy region provided a simply way to deal with the pressure and velocity boundary conditions on the interface of phase transformation.

References

[1] A. Sluzalec, Flow of metal undergoing laser irradiation, Numerical Heat Transfer 14 (1988) 253–263.
[2] N. Postacioglu, P. Kapadia, J. Dowden, A theoretical model of thermocapillary flows in laser welding, Journal Physics D: Applied Physics 24 (1991) 15–20.
[3] W. Sudnik, D. Rasdaj, W. Erofeew, Computerized simulation of laser beam welding, modeling and verification, Journal Physics D: Applied Physics 29 (1996) 2811–2817.
[4] J. Kroos, U. Gratzke, G. Simon, Towards a self-consistent model of the keyhole in penetration laser beam welding, Journal Physics D: Applied Physics 26 (1993) 474–480.
[5] R. Ducharme, K. Williams, P. Kapadia, J. Dowden, B. Steen, M. Glowacki, The laser welding of thin metal sheets: an integrated keyhole and weld pool model with supporting experiments, Journal Physics D: Applied Physics 27 (1994) 1619–1627.
[6] X.-h Ye, X. Chen, Three-dimensional modeling of heat transfer and fluid flow in laser full-penetration welding, Journal Physics D: Applied Physics 35 (2002) 1049–1056.
[7] C. Lampa, A.F.H. Kaplan, J. Powell, C. Magnusson, An analytical thermodynamic model of laser welding, Journal Physics D: Applied Physics 30 (1997) 1293–1299.
[8] R. Fabbro, K. Chouf, Dynamical description of the keyhole in deep penetration laser welding, Journal of Laser Applications 12 (2000) 142–148.
[9] P. Solana, J.L. Ocana, A mathematical model for penetration laser welding as a free boundary problem, Journal Physics D: Applied Physics 30 (1997) 1300–1313.
[10] C. Carmignani, R. Mares, G. Toselli, Transient finite element analysis of deep penetration laser welding process in a single-pass butt-welded thick steel plate, Computation Methods in Applied Mechanics and Engineering 179 (1999) 197–214.
[11] V.R. Volle, C. Prakash, A fixed grid numerical modeling methodology for convection diffusion mushy region phase-change problems, International Journal Heat Mass Transfer 30 (89) (1987) 1709–1719.
[12] M.M. Chen, Scooping Analyses and Limitation of Transport Phenomena Modeling for Laser Surface Modification [A]. Laser Processing Surface Treatment and Film Deposition [M], Kluwer Academic Publishers, New York, 1996.
[13] S.V. Pantankar, Numerical Heat Transfer and Fluid Flow, Hemisphere, Washington, DC, 1980.
[14] S. Majumdar, Role of underrelaxation in momentum interpolation for calculation of flow with nonstaggered grids, Numerical Heat Transfer 13 (1988) 125–132.